energies

MDPI

Article

Experimental Investigation of Permeability Sensitivity of Coal Reservoir to Reservoir Pressure and Its Fluid–Solid Coupling Control Mechanism

Xiaokai Xu [1,2,*], Yue Xin [1], Qingchao Li [1], Shuo Zhang [1], Lin Tian [3] and Zhengzheng Xue [1]

[1] School of Energy Science and Engineering, Henan Polytechnic University, Jiaozuo 454003, China; liqingchao2020@hpu.edu.cn (Q.L.)
[2] College of Geoscience and Surveying Engineering, China University of Mining & Technology (Beijing), Beijing 100083, China
[3] School of Resources and Environment, Henan Polytechnic University, Jiaozuo 454003, China
* Correspondence: xuxiaokai110110@163.com

Abstract

During coalbed methane (CBM) production, coal reservoir pore/fracture structure varies dynamically under the action of fluid–solid coupling. And coal reservoir permeability changes accordingly. In order to factually investigate the dynamic changes in coal reservoir permeability in the CBM well drainage process, a comparative simulation experiment on the difference in coal permeability sensitivity to confining pressure (external pressure) and pore pressure (internal pressure) was carried out in this study. The results show that coal permeability presents a typical negative exponential decline with a decrease in pore pressure. The pore pressure sensitivity experiment can effectively simulate the permeability sensitivity characteristics caused by coal reservoir pressure. Based on the negative exponential function relationship between permeability and effective stress, a new calculating method for the effective stress coefficient was deduced. Namely, its value could be expressed as the quotient of the pore pressure sensitivity curve regression coefficient divided by the confining pressure sensitivity curve regression coefficient. A dynamic theoretical model for coal reservoir permeability characterized by reservoir pressure was systematically constructed based on the unique fluid (gas/liquid)–solid coupling characteristics of coal reservoirs. Furthermore, the general characteristics of the stress sensitivity of coal permeability during coalbed methane (CBM) recovery were analyzed. The dynamic evolution characteristics of coal reservoir permeability in the study area were further examined. Taking the production and drainage data of a typical actual CBM production well as an example, the theories regarding the permeability sensitivity of coal reservoirs to reservoir pressure presented in this paper were validated in practice. This indirectly confirmed the rationality and accuracy of the calculation method for the effective stress coefficient obtained through laboratory-based permeability sensitivity simulation experiments. This research provides robust theoretical support for the systematic monitoring and prediction of fluid production, reservoir pressure, and permeability during the CBM production process, carrying significant practical implications.

Keywords: coal reservoir; permeability; reservoir pressure; stress sensitivity; effective stress coefficient; fluid–solid coupling

Check for updates

Academic Editor: Reza Rezaee

Received: 17 March 2026
Revised: 13 April 2026
Accepted: 15 April 2026
Published: 29 April 2026

Copyright: © 2026 by the authors. Licensee MDPI, Basel, Switzerland. This article is an open access article distributed under the terms and conditions of the Creative Commons Attribution (CC BY) license.

1. Introduction

As the global energy structure continues to evolve, exploration and production of coalbed methane (CBM)—an important unconventional gas resource—have expanded steadily [1]. Coal, found in CBM reservoirs, is a kind of typical organic sedimentary soft rock compared to the rock found in conventional natural gas reservoirs [2]. Its permeability is very sensitive to the stress environment [3–5]. In general, we use the stress sensitivity of permeability to evaluate the change in reservoir seepage ability in response to porous media deformation caused by a varying stress environment [6–9]. Correctly evaluating stress sensitivity for reservoir permeability has important roles in productivity analysis, proration adjustment and scheduling recovery. The stress or pressure environment of coal can be summarized into two types. One is external pressure, such as overburden stress and tectonic stress; the other is internal pressure, mainly including pore fluid pressure (namely, reservoir pressure). Coal reservoir permeability is relatively low in areas of large burial depth or high geostress [10]. However, it is generally believed that the external pressure is constant in CBM production. Reservoir pressure decreases as the fluids (water, gas) in the coal reservoir are removed. Permeability also declines, since the coal's fractures are compressed or closed [4,7,11], although this could be restrained to some extent by the matrix shrinkage effect later [12,13]. The stress sensitivity of a coal reservoir can usually be determined through a laboratory seepage mechanics experiment on core samples [4,7,9,14–16].

In general, stress sensitivity evaluation experiments are based on the principle of effective stress [17–24]. Effective stress is a kind of equivalent stress, whose mechanical behavior on the coal skeleton is exactly the same as that under the combined action of internal and external stresses. The initial effective stress form is the difference between external and internal stresses, namely, the Terzaghi effective stress. It was first put forward when Terzaghi conducted a study on a water-saturated soil medium [25]. Terzaghi's effective stress is also known as the classic effective stress. A stress sensitivity experiment usually has two kinds of control methods for effective stress: one is changing the confining pressure (external pressure) with a constant pore pressure (internal pressure), and the second is the opposite. To date, many scholars have carried out experimental studies on the stress sensitivity of coal reservoirs [3,13,26–29]. Because it is very easy to change the confining pressure in experiments, many researchers have evaluated permeability sensitivity to reservoir pressure in CBM production through confining pressure sensitivity experiments. This is based on Terzaghi's effective stress law. Specifically, a variation in confining pressure was viewed as equivalent to a variation in pore pressure (reservoir pressure) [3,29–31]. Some scholars have pointed out that stress sensitivity experiments with varying confining pressures cannot reflect the actual stress sensitivity characteristics caused by a decrease in reservoir pressure because their change mechanisms for effective stress are different [23,32–34].

In recent years, considerable efforts have been devoted to investigating the dynamic evolution of coal reservoir permeability during CBM production and to establishing corresponding permeability models. Previous studies indicate that permeability's evolution is strongly controlled by variations in reservoir pressure, effective stress, gas adsorption–desorption, and matrix deformation [35]. For instance, permeability models incorporating the coupled effects of effective stress and sorption-induced matrix shrinkage have been proposed to describe permeability changes during reservoir depletion, suggesting that permeability may initially decrease due to fracture compression and subsequently increase as a result of matrix shrinkage induced by gas desorption [36–38]. Analytical and semi-empirical models considering fracture deformation and adsorption-induced strain have also been developed to characterize permeability's evolution in coal reservoirs [38,39]. In addition, some studies have shown that coal permeability's evolution may be strongly

anisotropic because cleat structure, bedding, and sorption-induced deformation differ with direction. For example, Liu et al. developed a model linking gas sorption-induced changes in coal permeability to directional strains through a modulus reduction ratio [40], and recent work further established a fully anisotropic permeability model for coal considering stress sensitivity, anisotropic internal swelling/shrinkage, and gas rarefaction effects [41]. These studies indicate that sorption anisotropy may also play an important role in permeability evolution under reservoir depletion. Nevertheless, the existing studies still present several limitations: many models rely mainly on theoretical derivation or numerical simulation with limited experimental validation; moreover, the coupled influence of external loading stress and internal fluid pressure during reservoir pressure depletion is not fully considered. Consequently, the dynamic response mechanism of coal reservoir permeability to reservoir pressure decline remains insufficiently understood, highlighting the need for further experimental investigation and improved permeability modeling under realistic loading–seepage conditions.

To evaluate the sensitivity of coal reservoir permeability to reservoir pressure more objectively and realistically, it is essential to conduct specialized, in-depth research involving loading seepage experiments to investigate permeability sensitivity under external loading stress and internal fluid pressure. Based on a systematic analysis of the dynamic evolution of coal reservoir permeability with respect to reservoir pressure and the underlying fluid–solid coupling mechanisms, a mathematical–physical model was constructed to better reflect the inherent objective attributes of coal reservoirs.

Accordingly, this study designed a series of loading seepage experiments on coal rock to simulate fluid production and investigate the sensitivity characteristics of coal reservoir permeability to reservoir pressure. The control mechanisms governing the dynamic changes in coal reservoir permeability induced by reservoir pressure were examined, followed by the development of a theoretical model. Furthermore, the validity of the proposed model was verified using production data from actual coalbed methane (CBM) wells in the study area. This research aims to provide a fundamental theoretical basis for the systematic monitoring and prediction of coal reservoir pressure, permeability, and fluid production during CBM well operations.

2. Geological Background and Basic Physical Properties of Coal Reservoir

There are abundant coal and CBM resources in the Southern Qinshui Basin, where original permeability and reservoir reformation conditions are relatively good. It is accordingly regarded as one of the most prospective CBM fields currently under active development in China. In particular, the No. 3 coal seam of the Permian Shanxi Formation (P_1s) is the principal CBM reservoir from which coal samples were collected. The stratigraphy of the study area is characterized by typical Permian coal-bearing sequences, mainly including the Shanxi Formation (P_1s) and the underlying Taiyuan Formation (P_1t) [42]. The Taiyuan Formation consists of marine–continental transitional deposits, including limestone, mudstone, and coal seams, reflecting a transitional depositional environment. Overlying this unit, the Shanxi Formation is dominated by continental clastic deposits formed in a delta plain setting, and is composed mainly of sandstone, mudstone, and multiple coal seams. Among them, the No. 3 coal seam is the primary target for coalbed methane (CBM) development in the study area due to its favorable thickness, continuity, and gas-bearing properties. The coal seam in the study block from which the samples were collected has an average burial depth of approximately 500 m and an average thickness of 4.7 m. The regional geological structural characteristics and coal measure strata (P_1s) information of the study area are shown in Figure 1. Multi-stage plate movements governed not only the formation and evolution of the Qinshui Basin but also the structural and thermal evolution characteristics

of the associated coal-bearing strata [43]. Combined magmatic thermal metamorphism and dynamic metamorphism collectively facilitated the regional metamorphism of the No. 3 coal seam.

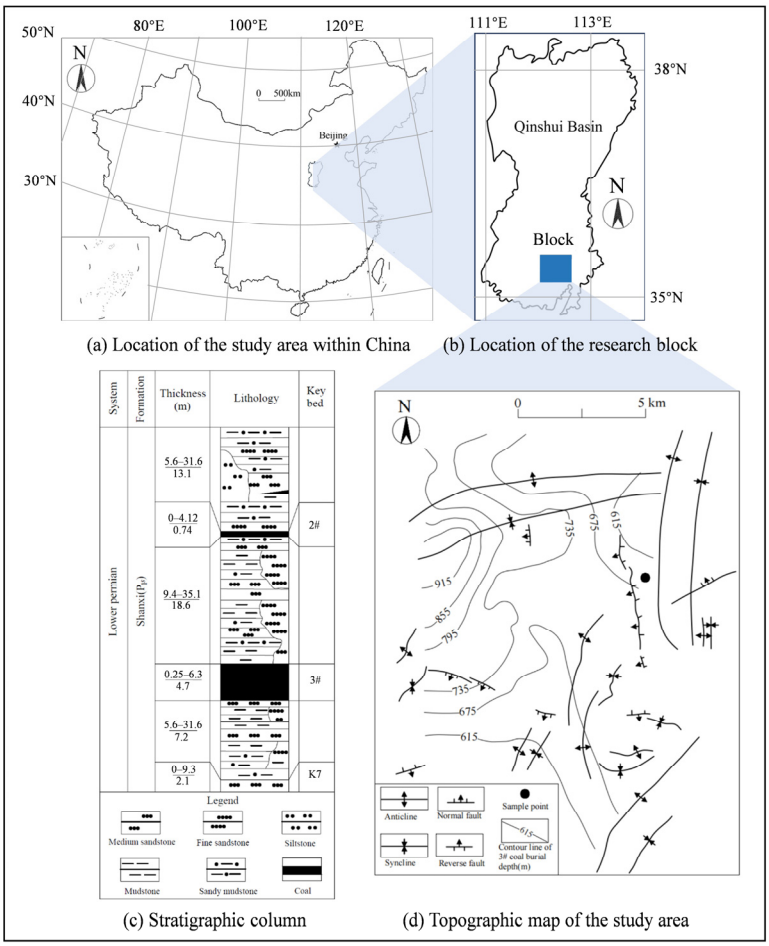


Figure 1. Geotectonic background and coal measure strata (P_1s) of the study area (revised according to [42,44]).

On the whole, the coal-forming environment of Shanxi Formation was a delta plain in this area. Its coal bearing strata have successively experienced Indosinian, Yanshanian and Himalayan tectonic movements. Among these, tectonic activity was relatively strong during the Yanshanian. Strong regional tectonic deformation occurred and was accompanied by strong intermediate-acid magma intrusion activities at the same time. A series of folds and faults at different levels were generated, as shown in Figure 1. Local abnormal thermal metamorphism caused by regional magmatic activity happened in the coal seam. Consequently, the degree of coal metamorphism is generally high, with anthracite coal comprising the dominant lithotype.

Its basic physical properties were measured, including density, vitrinite reflectance ($R_{o,max}$), coal macerals and proximate analysis. And the results are shown in Table 1. These findings indicate that the region is a typical high-rank coal (anthracite) area for CBM exploration and development. It is evident that the Permian coal measure strata have undergone multi-stage tectonic movements, resulting in a high degree of thermal evolution.

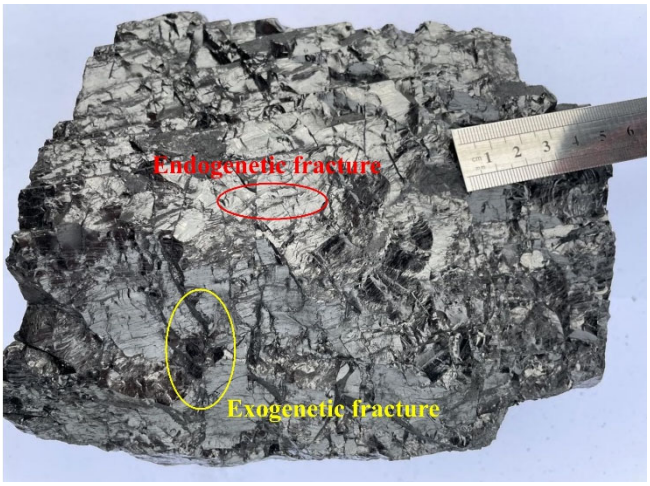
Table 1. Basic physical properties of coal.

Density /g/cm^3	$R_{o,max}$ /%	Coal Maceral Content/%			Proximate Analysis/%		
		Vitrinite	Inertinite	Clay	Moisture	Ash	Volatiles
1.44	2.4	86.86	6.166	7.775	0.68	11.78	5.92

The collected raw coal with clearly visible beddings, cleats and fractures is shown in Figure 2a. It can also be observed through scanning electron microscopy (SEM) that there are developed micro-fractures in the coal matrix, as shown in Figure 2b. So, the research coal could be regarded as a typical pore–fracture double porosity reservoir [45,46]. These fractures (networks) determine the permeability of coal [14,47]. Several coal cylinders were drilled along the direction parallel to the bedding from one big coal block, and were processed into normal cylindrical samples, as shown in Figure 2c. Sample pretreatment for the experiment was in accordance with the Chinese Petroleum Industry Standard [48]. Four coal cylinders with no macro-fractures were selected: two of them were used for confining pressure sensitivity experiments, and the other two for pore pressure sensitivity experiments. The details of the coal cylinders are shown in Table 2. It can be seen that the physical properties of the four samples are of good consistency. To minimize the influence of coal heterogeneity, all samples used in this study were prepared as parallel specimens from the same coal block. Prior to the experiments, ultrasonic wave velocity tests were conducted to evaluate the internal structural consistency of the samples. The results showed that the wave velocities of the selected specimens are highly similar, indicating comparable internal structures and mechanical properties. Therefore, the selected samples can be considered representative for the experimental analysis. This approach is commonly adopted in coal permeability experiments to ensure comparability between samples.

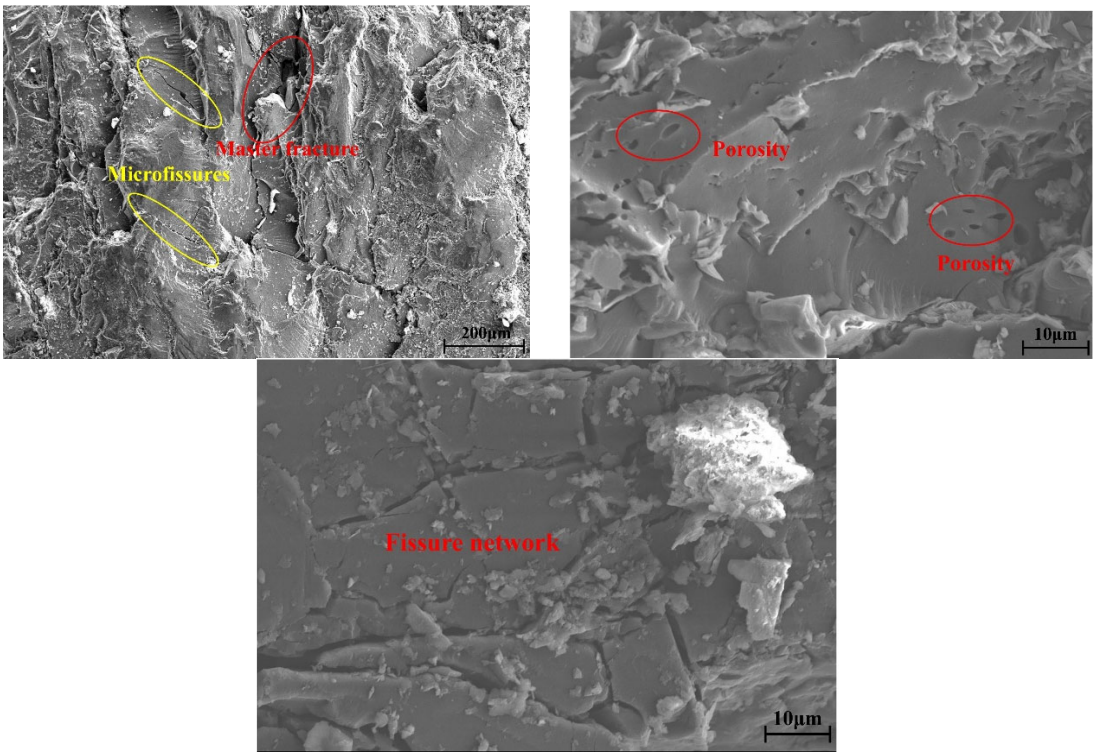
Table 2. The details of selected coal cylinders.

Experiments	Sample ID	Diameter/cm	Length/cm	Density/g/cm^3	Porosity/%
Confining pressure	S1	2.50	5.03	1.42	5.24
	S2	2.51	5.00	1.45	4.38
Pore pressure	S3	2.51	5.02	1.45	4.38
	S4	2.50	4.98	1.46	4.17

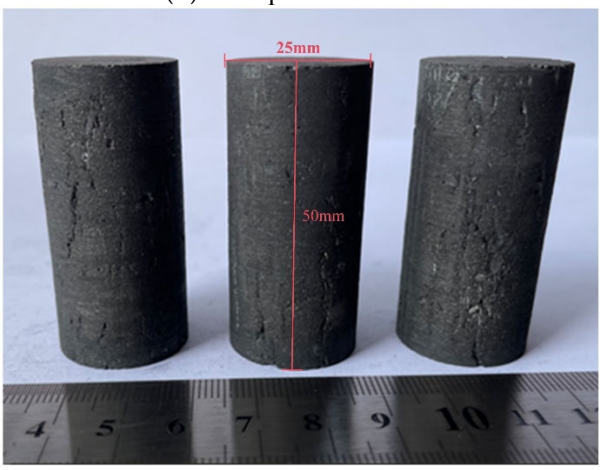


(**a**) Macroscopic coal

Figure 2. *Cont.*



(**b**) SEM picture of coal



(**c**) Processed cylinders

Figure 2. Coal samples.

3. Experimental Procedure

3.1. Confining Pressure Sensitivity Experiments

Confining pressure sensitivity experiments were conducted using the PoroPDP-200 permeability instrument (Core Laboratories, Jiaozuo, China). Permeability was measured through the pulse attenuation method [27,49,50]. We chose nitrogen of a purity of 99.999% as the test gas, with which the matrix shrinkage effect could be minimized with respect to CH_4 and CO_2 [51,52].

The test pressure p (pore pressure) was set to 2.0 MPa. The confining pressure was then incrementally increased to 5.0, 6.0, 7.0, 8.0, 9.0, and 10.0 MPa, and permeability was measured at each step.

3.2. Pore Pressure Sensitivity Experiments

It is difficult to control pore pressure with respect to the confining pressure. There are two ways to change pore pressure. One is to change the injection pressure, the gas pressure at the inlet, to control the coal's upstream gas pressure [7,21,53]; the other way is to change the back pressure, the gas pressure at the outlet, to control the coal's downstream gas pressure [17,54]. In the actual CBM development process, the overburden pressure of the coal reservoir could be generally regarded as a constant [55]. As fluids (gas, water) are produced, coal reservoir pressure near the wellbore begins to drop and gradually presents a funnel-shaped distribution. Therefore, the back pressure sensitivity experiment may be more suitable for simulating the seepage characteristics of reservoir fluids in CBM production [56–58]. So, the method of changing back pressure was used in this pore pressure sensitivity experiment.

The integrated reservoir damage analyzer (LSY-1A, Haian Oil, Haian, China) was applied in this experiment. Its unit structure is shown in Figure 3. The instrument mainly consists of three parts. The first part is the high-pressure gas source, including the driving pressure pump and high-pressure tank; the second part mainly includes the core holder, thermostat and control device of confining pressure; the third part is the back pressure control part, mainly including the back pressure pump. The high-purity nitrogen gas was still used as the test fluid medium, and the gas injection pattern was set as constant pressure injection.

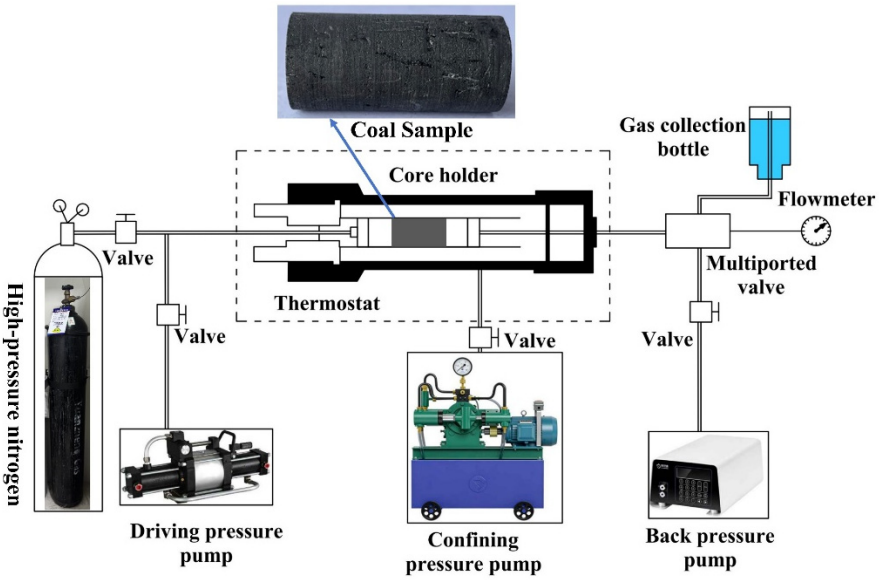


Figure 3. Experimental apparatus structure schematic diagram.

The specific experimental procedures are as follows:

(1) First, load the confining pressure to 2.0 MPa. Then, gradually inject N_2 into the coal sample until the pore pressure reaches the original reservoir pressure (P, 5.0 MPa). Meanwhile, raise the confining pressure synchronously and keep it 2 MPa higher than the pore pressure throughout. Afterwards, maintain the pore pressure at 5.0 MPa and the confining pressure at 7.0 MPa for about 24 h to make the gas saturated and the pressure balanced.

(2) Gradually lower the back pressure (p) to several set points (4.98, 4.7, 4.5, 4.0, 3.0, 2.0 and 1.0 MPa). Keep each back pressure point invariable for 0.5 h and record the value of steady flow. Finally, calculate the permeability (k) of the coal sample at each point using the steady-state method [7,26,53].

4. Results

4.1. Confining Pressure Sensitivity

In the confining pressure sensitivity experiment, the difference between confining pressure (p_c) and pore pressure (p_p) is regarded as the effective stress. The permeability measured at the initial confining pressure p_{c0} (5.0 MPa) is denoted as the initial permeability (k_0). Furthermore, we can get dimensionless effective stress σ ($\frac{p_c - p_p}{p_{c0} - p_p}$) and permeability ($\frac{k}{k_0}$) through normalization processing. Due to the positive linear relationship between confining pressure (p_c) and dimensionless effective stress (σ), the increase in σ indicates a rise in p_c. The experimental results for the confining pressure sensitivity are shown in Figure 4.

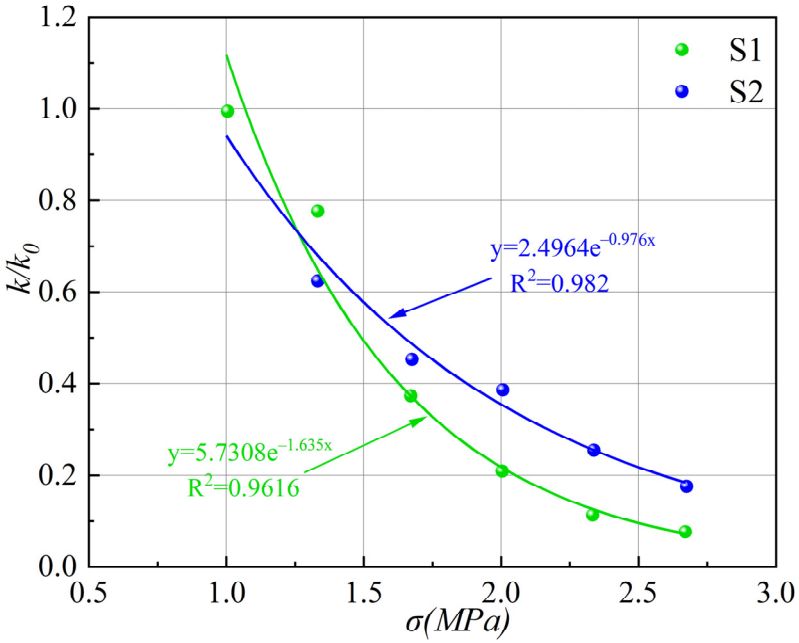


Figure 4. Confining pressure sensitivity curves.

In Figure 4, it can be observed that there is an obvious negative exponential function relationship between k/k_0 and σ. k/k_0 decreases with the increase in σ (or p_c) as a whole. At the early stage of effective stress increase, coal permeability declines rapidly; the decline rate slows down in the later stage. This complies with the general rule of stress sensitivity of coal permeability [29,53,59,60].

Coal, a typical organic sedimentary rock, is extremely sensitive to stress. However, there is not a unified method for stress sensitivity evaluation for coal reservoirs. Here, we evaluate its stress sensitivity degree according to the Chinese Petroleum Industry Standard [61]. The rate of permeability change caused by stress sensitivity can be defined as

$$D = \frac{k_0 - k_i}{k_0} \times 100\% \quad (1)$$

where D is the rate of permeability change, %; and k_i is the permeability under the (i)th stress state, $\times 10^{-3}$ μm^2.

The permeability damage rate (D_{max}) is defined as the maximum rate of permeability change. The permeability damage evaluation index system is shown in Table 3. The calculated permeability damage rate for coal confining pressure sensitivity is more than 80%. So, it has reached the "Strong" level of permeability damage.

Table 3. Stress sensitivity damage evaluation index of permeability.

Permeability Damage Rate	Damage Level
$D_{max} \leq 5\%$	None
$5\% < D_{max} \leq 30\%$	Weak
$30\% < D_{max} \leq 50\%$	Mid-weak
$50\% < D_{max} \leq 70\%$	Mid-strong
$D_{max} > 70\%$	Strong

4.2. Pore Gas Pressure Sensitivity

In pore pressure sensitivity experiments, permeability damage mainly occurs on the back pressure control side of the coal sample, so the difference between the confining pressure (p_c) and the back pressure (p_b) can be viewed as the effective stress. The initial permeability (k_0) was measured at the initial back pressure p_{b0} (4.98 MPa). After normalization processing, the dimensionless effective stress (σ) and permeability can be expressed as $\frac{p_c - p_b}{p_c - p_{b0}}$ and $\frac{k}{k_0}$, respectively. We can see that a decrease in p_b indicates a linear increase in σ. It is worth noting that the conceptions of the initial state, dimensionless effective stress and permeability used here are different from those defined in the confining pressure sensitivity experiment. The experimental results for pore pressure sensitivity are shown in Figure 5.

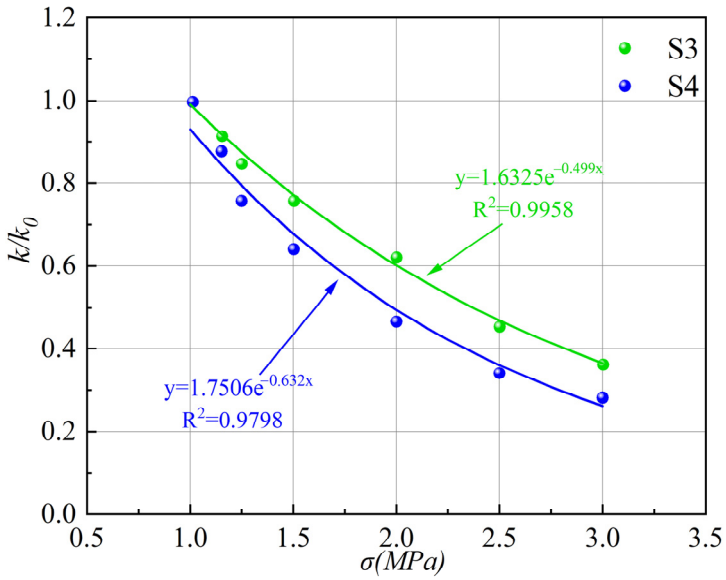


Figure 5. Pore pressure sensitivity curves.

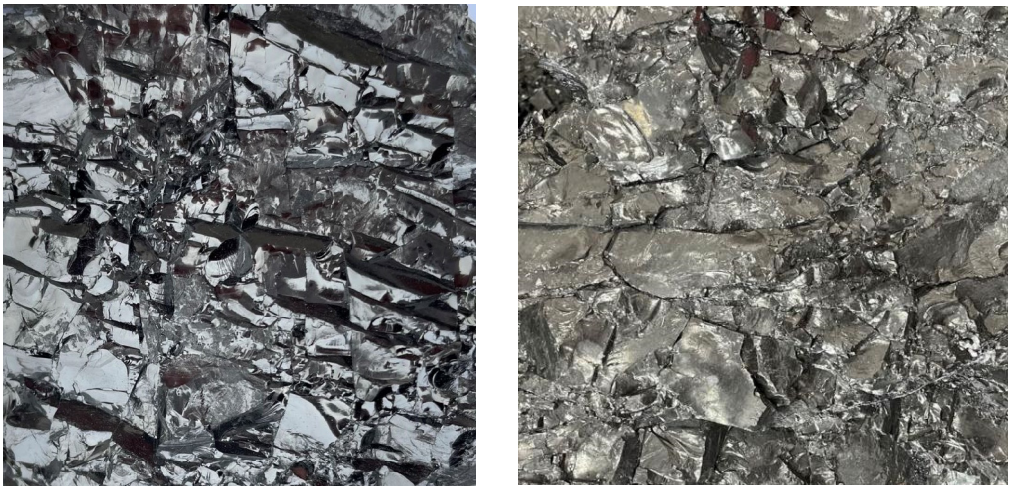
From Figure 5, it can also be observed that k/k_0 declines in a good exponential form with the increase in σ as a whole. The calculated permeability damage rates for coal pore pressure sensitivity are approximately 64.0% for sample S3 and 72.0% for sample S4, indicating a "Mid-strong" level of permeability damage according to Table 3.

5. Theoretical Model for Coal Permeability Sensitivity and Mechanism Analysis

5.1. Special Gas–Solid Coupling Mode—Shrinkage Effect of Coal Matrix

According to the principles of surface physicochemistry, molecules or atoms on a solid surface experience unbalanced forces and therefore possess additional Gibbs free energy compared with molecules within the interior, which is referred to as surface Gibbs free energy (surface energy). Its magnitude can be interpreted as the work required to increase the unit surface area of a solid. Based on the principle of minimum energy, the Gibbs

surface free energy of a solid tends to decrease spontaneously. Because the solid surface cannot easily contract, the reduction in surface energy can only be achieved through the adsorption of gas-phase or liquid-phase molecules. Coal, a typical organic rock, possesses a well-developed pore–fracture system and an enormous specific surface area. Therefore, it exhibits a strong adsorption capacity for methane molecules, which is the most important characteristic of coal reservoirs as unconventional natural gas reservoirs. Coal reservoirs exhibit a typical dual pore–fracture structure composed of matrix pores and fractures, as shown in Figure 6. It is generally considered that pores ranging from nanometer to micrometer scales are widely developed within the matrix and constitute the primary storage space for adsorbed CBM. The cleat fracture system between the matrix frameworks serves as the principal pathway for gas seepage.



(**a**) Bright coal section. (**b**) Dull coal section.

Figure 6. Macroscopic matrix–cleat fracture structure of the raw coal sample.

After gas molecules are adsorbed on the pore surfaces of coal, the attractive force between surface molecules of the coal skeleton and internal molecules weakens. As a result, the intermolecular distance increases, leading to volumetric expansion of the coal matrix blocks. Conversely, during gas desorption, the coal undergoes shrinkage deformation. This phenomenon represents the most distinctive gas–solid coupling behavior in coal reservoirs. The adsorption-induced swelling deformation of coal has been confirmed by numerous experimental observations [62,63].

After gas adsorption on the pore surfaces within the coal matrix, the surface energy decreases and the coal matrix undergoes expansion deformation. Meanwhile, the cleat fractures between the matrix frameworks shrink, leading to a synchronous reduction in gas permeability. Because adsorption and desorption are mutually inverse processes, adsorption-induced swelling deformation is also the inverse process of desorption-induced shrinkage deformation. During gas desorption, shrinkage deformation of the coal matrix occurs. This increases the width of cleat fractures and enhances permeability. In this study, the term "adsorption swelling effect" is equivalent to the "desorption shrinkage effect," and the two terms are used interchangeably without distinction.

The adsorption of methane by coal generally follows the characteristics of a Type I adsorption isotherm. The relationship between gas adsorption capacity and gas pressure can generally be described by the Langmuir equation in Equation (2) [64].

$$V = \frac{abp}{1 + bp} = \frac{V_L p}{P_L + p} \tag{2}$$

In the equation, p represents the gas adsorption equilibrium pressure (MPa). V denotes the gas adsorption capacity corresponding to pressure p (m^3/t). V_L or a represents the Langmuir volume, indicating the maximum adsorption capacity of coal for methane (m^3/t). $P_L = 1/b$ is the Langmuir pressure, representing the gas pressure corresponding to half of the V_L adsorption capacity (MPa).

Numerous scholars have conducted stress–strain experiments on coal under different pore gas pressures. These studies have shown that the relationship between coal desorption-induced volumetric shrinkage strain and pore pressure also generally follows the form of the Langmuir equation as in Equation (3) [62,65].

$$\varepsilon_s = \frac{\varepsilon_{\max} p}{p + p_{50}} \tag{3}$$

In the equation, ε_s represents the volumetric expansion strain of the coal matrix at gas pressure p. ε_{max} denotes the Langmuir volumetric strain, which is the ultimate strain under an infinitely large gas pressure. p_{50} represents the gas pressure corresponding to half of the Langmuir volumetric strain (MPa).

Currently, most theoretical calculation methods for adsorption swelling strain in coal are based on Bangham theory. After gas adsorption on the coal surface, the surface energy decreases. Bangham and co-workers proposed that the reduction in surface energy is proportional to the linear adsorption swelling strain of coal as in Equation (4).

$$\varepsilon_l = \frac{\Delta l}{l} = \gamma \pi \tag{4}$$

In the equation, ε_l represents the linear adsorption swelling strain of coal. γ is the deformation constant, which depends on the physical properties of coal. π denotes the change in surface tension, also known as the surface pressure, with units of N/m, and its direction is parallel to the surface.

According to the Gibbs [66] adsorption equation, the following relationship can be obtained.

$$\pi = \int_0^p \frac{V}{V_m S} RT d(\ln p) \tag{5}$$

In this equation, V represents the gas adsorption capacity of coal (m^3/t). V_m is the molar volume of gas, equal to 22.4 L/mol. S represents the specific surface area of coal. R is the universal gas constant. T denotes the absolute temperature (K). p represents the gas pressure (MPa).

Maggs proposed a relationship between the deformation constant γ and the physical and mechanical properties of coal.

$$\gamma = \frac{S\rho}{E_A} \tag{6}$$

In this relationship, ρ represents the apparent density of coal (t/m^3). E_A denotes the adsorption swelling modulus of coal (MPa). This modulus is not necessarily equal to the elastic modulus E. For coal, the elastic modulus E is generally greater than E_A. The ratio between them typically ranges from 2 to 11. E_A is a parameter that is difficult to determine and depends on the assumed geometric structure model of coal.

Yate [66] further provided a more specific expression for γ.

$$\gamma = \frac{2S\rho}{9K} = \frac{2S\rho(1-2\nu)}{3E} \tag{7}$$

In this equation, K represents the bulk modulus of coal (MPa). E represents the elastic modulus of coal (MPa). ν denotes Poisson's ratio.

Substituting Equations (5) and (7) into Equation (4) yields the following result.

$$\varepsilon_l = \frac{2\rho(1-2\nu)RT}{3EV_m}\int_0^p V d(\ln p) \tag{8}$$

Furthermore, substituting the Langmuir equation in Equation (2) into Equation (8) gives the theoretical linear strain ε_l of coal adsorption swelling.

$$\varepsilon_l = \frac{2a\rho(1-2\nu)RT}{3EV_m}\int_0^p \frac{b}{1+bp}dp = \frac{2a\rho(1-2\nu)RT}{3EV_m}\ln(1+bp) \tag{9}$$

The theoretical volumetric strain ε_s of coal adsorption swelling can then be expressed accordingly.

$$\varepsilon_s = 3\varepsilon_l = \frac{2a\rho(1-2\nu)RT}{EV_m}\ln(1+bp) \tag{10}$$

The above equation represents the thermodynamic theoretical calculation formula for coal adsorption swelling strain derived from Bangham theory. In this equation, the adsorption constants a and b can be obtained from isothermal adsorption experiments on coal. The elastic modulus E and Poisson's ratio ν can be determined from conventional mechanical experiments on coal and rock. The adsorption swelling strain model theoretically reveals the relationship between coal deformation during adsorption swelling and its physical and mechanical properties. The parameters in the model have clear physical meanings and are relatively easy to obtain. From the derivation of the stress–strain constitutive model for coal adsorption swelling, it can be seen that the shrinkage effect of the coal matrix induced by gas desorption is one of the most significant characteristics of coal rock fluid–solid coupling.

Because adsorption and desorption are mutually inverse processes, and the fluid–solid coupling problem in coal reservoirs is generally assumed to remain within the elastic range, adsorption swelling deformation and desorption shrinkage deformation are considered to be completely reversible processes. Therefore, the study of adsorption swelling effects is equally applicable to the desorption shrinkage process in coal.

Although stress–strain experiments of adsorption swelling in coal samples can objectively reflect the stress–strain characteristics of coal rock, the complexity of experiments and the discreteness of samples limit their application. Therefore, when studying the changes in coal porosity and permeability caused by matrix shrinkage, it is relatively simple to use the above model to describe the relationship between desorption shrinkage strain and gas pressure.

5.2. Dynamic Permeability Model of Coal Reservoir

Coal reservoirs possess a typical dual pore–fracture structure composed of matrix pores and fractures. It is generally believed that the permeability within the matrix pores is extremely low, and that the cleat fracture system between the matrix frameworks plays the dominant role in seepage. Some researchers [67] have abstracted coal as a bundled matchstick geometric model, as shown in Figure 7. In this model, the cylindrical bodies represent the coal matrix framework, while the spaces between the cylinders correspond to the cleat fractures between matrix blocks. This geometric model has been widely used in the modeling of coal permeability.

Numerous scholars have conducted extensive experimental studies on the stress sensitivity of coal permeability. It is generally accepted that as reservoir pressure (pore water pressure or gas pressure) decreases, the effective stress borne by the coal skeleton increases. Consequently, the cleat fractures tend to compress and close, and the permeability of coal rock decreases according to a negative exponential law. This behavior has also been confirmed by the experimental results of this study. Based on coal rock mechanical seepage

experiments, Seidle [67] and co-workers summarized a classical exponential relationship between coal permeability (k) and effective stress (σ), as shown in Equation (11).

$$k = k_0 e^{-3c_f(\sigma-\sigma_0)} \tag{11}$$

In this model, σ_0 represents the initial effective stress perpendicular to the cleat fracture surface (MPa). k_0 denotes the initial fracture permeability. c_f represents the fracture volumetric compressibility coefficient (MPa^{-1}), which can be obtained by fitting experimental data.

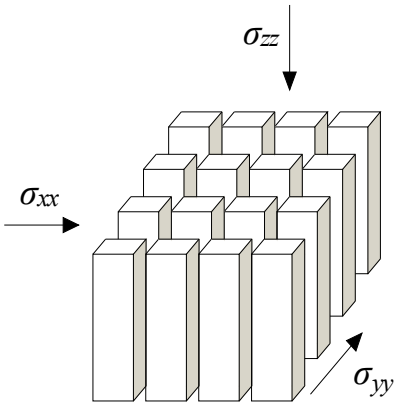


Figure 7. A bundled matchstick geometry model of coal [67].

In general porous media underground, the fluid–solid coupling mainly manifests as the relatively simple pressure effect exerted by pore fluids on the solid skeleton of the porous medium. This effect is commonly represented by pore fluid pressure. For example, in conventional sandstone reservoirs, groundwater and natural gas exert pressure within pore spaces. However, in coalbed methane systems, in addition to the basic fluid pressure effect between methane and the coal skeleton, there exists another distinctive gas–solid coupling mechanism known as the adsorption swelling effect. This mechanism has already been described in Section 5.1.

It should be noted that the gas adsorption capacity of the coal matrix and the microscopic adsorption pores within the matrix are generally considered to be nearly unaffected by external forces [68]. Therefore, the overall expansion or shrinkage deformation of coal matrix blocks induced by gas adsorption or desorption can be regarded as an equivalent force acting on the surface of the entire matrix framework (i.e., the cleat fracture walls). This equivalent force is denoted as p_{ad}. The specific form of this adsorption-induced equivalent force p_{ad} can be derived from Equation (9). Its magnitude is positively correlated with gas pressure p, but mechanically it exhibits the characteristics of tensile stress. As gas pressure increases, the equivalent adsorption tensile stress also increases. This effect makes the effective stress mechanism of the coal matrix framework more complex. The combined effects of the gas adsorption equivalent force p_{ad} and the gas pressure p control the variation in effective stress within the gas-bearing coal matrix framework. This in turn governs the opening and closing behavior of cleat fractures confined by the coal matrix framework. Consequently, permeability changes simultaneously.

Considering the similarity between the stress–strain behavior of gas adsorption swelling and thermal expansion in coal matrices, Shi [38] and co-workers derived the effective stress–strain relationship during gas adsorption swelling in coal reservoirs. This derivation was based on the stress–strain relationship of homogeneous isotropic thermoelastic porous media. Using an analogy method, they derived the relationship under uniaxial linear elastic strain conditions, as expressed in Equation (12). In this equation, the first term

on the right-hand side represents the change in effective stress caused by the compressive effect of basic fluid pressure. The second term represents the change in effective stress caused by matrix shrinkage. This term corresponds to the effective stress variation induced by the adsorption-equivalent tensile stress p_{ad}.

$$\sigma - \sigma_0 = -\frac{\nu}{1-\nu}(p - p_0) + \frac{E}{3(1-\nu)}(\varepsilon_s - \varepsilon_{s0}) \tag{12}$$

In the equation, σ denotes effective stress. p represents pore fluid pressure. ε_s denotes the macroscopic volumetric strain caused by adsorption swelling. σ_0, p_0, and ε_{s0} represent the initial values corresponding to σ, p, and ε_s, respectively. E represents the elastic modulus. ν denotes Poisson's ratio.

The relationship between the isothermal adsorption swelling strain ε_s and gas pressure p can be effectively described by a Langmuir-type equation as shown in Equation (3). Substituting the Langmuir model for adsorption swelling into Equation (12) yields the relationship between effective stress σ and pore pressure p as shown in Equation (13).

$$\sigma - \sigma_0 = -\frac{\nu}{1-\nu}(p - p_0) + \frac{E\varepsilon_{\max}}{3(1-\nu)}\left(\frac{p}{p + p_{50}} - \frac{p_0}{p_0 + p_{50}}\right) \tag{13}$$

During the early stage of dewatering and pressure reduction in CBM wells, before reservoir pressure declines to the critical desorption pressure p_{cd}, large-scale methane desorption does not occur. Under these conditions, it can be assumed that only a single groundwater fluid exists within the cleat fractures of the coal reservoir. Alternatively, the coal may contain only a single inert gas such as helium (*He*). Helium does not undergo any physicochemical reaction with the coal matrix surface and therefore does not produce gas adsorption. Under these conditions, the fluid–solid coupling does not involve desorption-induced shrinkage deformation. Therefore, the stress–strain term associated with matrix shrinkage does not exist. Consequently, the change in effective stress in coal is caused solely by the compressive effect of basic fluid pressure.

$$\sigma - \sigma_0 = -\frac{\nu}{1-\nu}(p - p_0) \tag{14}$$

Combining the classical exponential relationship between coal permeability and effective stress yields a widely used permeability analysis model for gas-bearing coal, as shown in Equation (11). This model is referred to as the S–D model.

$$k = \begin{cases} k_0 \exp\left(3c_f \frac{\nu(p-p_0)}{1-\nu}\right) (p_{cd} \le p \le p_0) \\ k_0 \exp\left(3c_f \left(\frac{\nu(p-p_0)}{1-\nu} - \frac{E\varepsilon_{\max}}{3(1-\nu)}\left(\frac{p}{p+p_{50}} - \frac{p_{cd}}{p_{cd}+p_{50}}\right)\right)\right) (0 \le p \le p_{cd}) \end{cases} \tag{15}$$

In this model, p_{cd} represents the critical desorption pressure of the coal reservoir. k_0 represents the initial cleat fracture permeability of the coal reservoir. $\varepsilon_{\max}$ denotes the Langmuir volumetric strain. p_{50} represents the gas pressure corresponding to half of the Langmuir volumetric strain.

In the S–D model, the effective stress adopts the Terzaghi effective stress form. In other words, the effective stress coefficient is assumed to be equal to 1. However, the effective stress mechanism in coal is more complex. Therefore, the authors propose replacing the Terzaghi effective stress in the S–D model with a more general effective stress formulation. In addition, the adsorption swelling volumetric strain used in the S–D model is obtained from adsorption swelling stress–strain experiments. However, these experiments are complex and the macroscopic cleat fractures vary greatly among different coal samples. As a result, the experimental results exhibit large dispersion and lack representativeness.

Therefore, the authors propose replacing the adsorption swelling volumetric strain term in the S–D model with the thermodynamic theoretical model of adsorption swelling strain described earlier in Section 4.1. Although this thermodynamic model requires the adsorption constants a and b, these parameters can be obtained from methane isothermal adsorption experiments on coal. Such experiments are relatively simple to perform. Moreover, the use of powdered samples eliminates the heterogeneity and discreteness problems associated with coal samples. Therefore, the calculated results are more representative. Based on these considerations, the S–D model was improved. The resulting dynamic effective stress model and dynamic permeability theoretical model for coal reservoirs during CBM production are given in Equations (16) and (17), respectively.

$$\sigma - \sigma_0 = \begin{cases} -\frac{\alpha\nu(p-p_0)}{1-\nu}(p_{cd} \le p \le p_0) \\ -\frac{\alpha\nu(p-p_0)}{1-\nu} + \frac{2a\rho RT(1-2\nu)}{3(1-\nu)V_m}\ln\frac{1+bp}{1+bp_{cd}}(0 \le p \le p_{cd}) \end{cases} \tag{16}$$

$$k = \begin{cases} k_0 \exp\left(3c_f\frac{\alpha\nu(p-p_0)}{1-\nu}\right)(p_{cd} \le p \le p_0) \\ k_0 \exp\left(3c_f\left(\frac{\alpha\nu(p-p_0)}{1-\nu} - \frac{2a\rho RT(1-2\nu)}{3(1-\nu)V_m}\ln\frac{1+bp}{1+bp_{cd}}\right)\right)(0 \le p \le p_{cd}) \end{cases} \tag{17}$$

In these equations, the effective stress coefficient is denoted by α. ρ represents the apparent density of coal (t/m^3). a and b are adsorption constants. The remaining symbols have the same meanings as previously defined. Palmer [36] and co-workers proposed a simplified expression for the compressibility coefficient of cleat fractures. This usington neglects both the compressibility of matrix particles and the influence of matrix shrinkage on the primary seepage fractures.

$$c_f = \frac{(1+\nu)(1-2\nu)}{(1-\nu)\phi_{f0}E} \tag{18}$$

In this equation, ϕ_{f0} represents the initial porosity of the flow-conducting cleat fractures.

It should be emphasized that gas-bearing coal reservoirs during CBM production are generally considered to remain in the elastic deformation stage. The permeability model presented here is therefore based on the assumption of linear elastic deformation of gas-bearing coal rock. The adsorption constants a and b in the model can be obtained from methane isothermal adsorption experiments. The parameters c_f, ν, and E can be determined from conventional mechanical seepage experiments on coal rock. The effective stress coefficient α is the key parameter reflecting the effective stress mechanism under gas–coal coupling conditions. Its determination method based on permeability sensitivity experiments is presented in Section 6.3. Theoretically, α represents the ratio between the area on which fluid acts and the total area of a given cross-section. In practice, however, the complex gas–solid coupling mechanisms in coal make it difficult to theoretically calculate or experimentally determine the exact value of this coefficient. This study proposes a new method for calculating the effective stress coefficient based on comparative pressure sensitivity experiments of coal permeability. The detailed theoretical derivation is presented in Section 6.2.

5.3. General Analysis on Stress Sensitivity of Coal Permeability During CBM Recovery

The stress sensitivity of reservoir permeability is determined by its basic physical properties, such as material composition, pore/fracture structure and gas–solid coupling mechanical properties. So, it is the inherent nature of the reservoir. Its essence is that the pore/fracture structure varies with effective stress conditions, and then permeability is influenced. If only simple fluid pressure effects are considered, such as in conventional sandstone reservoirs, the effective stress increases as the production fluid pressure de-

creases. In the early stage of the effective stress increase, the seepage pore/fracture is easy to compress, which makes permeability show greater stress sensitivity damage. Later, the pore/fracture is difficult to compress further due to its relatively high degree of compaction, so the stress sensitivity is gradually weakened. Therefore, in subsurface porous media reservoirs, permeability generally exhibits a negative exponential decay pattern as reservoir pressure decreases [59,60]. However, in coal reservoirs, a special gas–solid coupling mechanism—the shrinkage effect of the coal matrix—exists. During CBM production, as pore pressure p declines, the adsorption-induced equivalent tensile stress p_{ad} also diminishes. The combined action of these two factors makes the evolution of the total effective stress more complex. Consequently, the stress sensitivity behavior of permeability becomes difficult to determine. Nevertheless, the adsorption-induced equivalent tensile stress p_{ad} reduces the increase in total effective stress under a unit pressure drop, thereby slowing the decline of permeability. At later stages characterized by low or ultra-low gas pressure, the total effective stress may even transition to a decreasing trend, and permeability may begin to increase, as shown in Figure 8. Based on the above gas–solid coupling analysis of coal and the mechanical theoretical model describing the dynamic permeability evolution of CBM coal reservoirs, the stress sensitivity of permeability during CBM production in a specific study area can be analyzed theoretically.

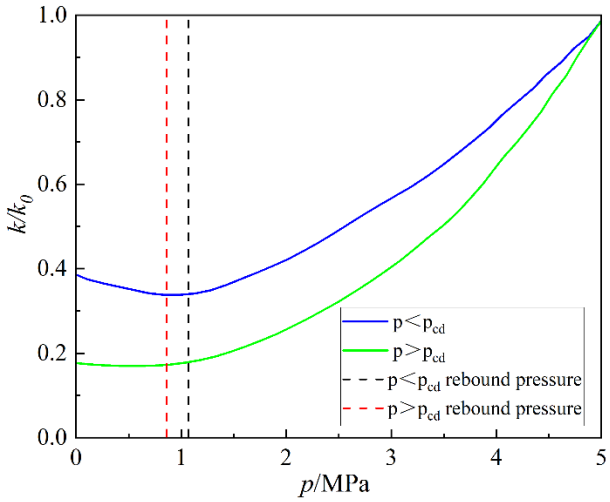


Figure 8. *k*-*p* curves of 3# coal reservoir.

It should be noted that the stress sensitivity of coal permeability in CBM reservoirs is essentially controlled by the tendency of the cleat fracture system, which dominates fluid flow, to close with increasing total effective stress. Therefore, coal permeability generally decreases exponentially with increasing effective stress, as described by Equation (11). However, during CBM production, the specific manifestation of permeability stress sensitivity depends on the evolution trend of the total effective stress under complex gas–solid coupling control, as shown in Equation (16).

Nevertheless, numerous experimental studies simulating actual CBM production conditions indicate that permeability generally still follows a negative exponential decline as the fluid pressure of coal samples decreases. The pore pressure sensitivity experiment conducted in this study, as shown in Figure 5, also demonstrates that the total effective stress in the current CBM reservoir conditions generally exhibits an increasing trend. Combined with the adsorption expansion–deformation curve of coal and Equation (16), it can be inferred that, during CBM production, while pore pressure decreases, the adsorption-induced equivalent tensile stress weakens and matrix shrinkage caused by desorption becomes stronger. The influence of adsorption-induced equivalent tensile stress on total

effective stress becomes significant only under low-pore-pressure conditions. Thus, at a certain reservoir pressure within the low-pressure to ultra-low-pressure range, the total effective stress acting on the main flow-controlling fracture system may reach a maximum value. At this point, permeability reaches its minimum value. The corresponding fluid pressure is referred to by some researchers as the rebound pressure p_{rb} [38]. After passing p_{rb}, the total effective stress begins to decrease, and permeability rebounds and increases. However, this phenomenon generally occurs only in the late production stage characterized by low or ultra-low reservoir pressure. In actual CBM wells, when the reservoir pressure approaches the depletion pressure, permeability usually remains at a relatively low level. This explains why many laboratory experiments simulating reservoir conditions show that permeability still follows a monotonically decreasing negative exponential trend as fluid pressure decreases, without observable rebound.

6. Discussions

6.1. Analysis of Simulative Experimental Results on Stress Sensitivity of Coal Permeability

In view of the fact that the experimental apparatus and test methods can only simulate the stress state of coal in the laboratory within a certain range of total effective stress (below coal's yield strength), there exists comparability between confining pressure sensitivity and fluid pressure sensitivity for the same kind of coal, which has nothing to do with the experimental instruments and methods applied to simulate a certain testing loaded state. Based on the above experimental results, it can be seen that permeability's sensitivity to the confining pressure is generally stronger than that to the fluid pressure. Permeability damage caused by confining pressure sensitivity is more serious than that caused by fluid pressure sensitivity by one grade.

In addition, from a general mechanistic perspective, permeability sensitivity under a non-adsorbing or weakly adsorbing gas is expected to be stronger than that under adsorbing methane. However, the present study did not perform a direct paired comparison between He and CH_4 using parallel specimens from the same batch; therefore, this point should be regarded as a qualitative interpretation rather than a direct quantitative conclusion of this work.

If the stress environment or its variation trend changes, the form of coal stress sensitivity would be different. Coal matrix skeleton deformation is controlled by the total effective stress. The Terzaghi effective stress (${\sigma_{\text{eff}}}^{\text{T}}$, see Equation (19)) has sufficient accuracy in research on loose porous media, such as saturated soil. But its applicability to complex oil/gas reservoirs has always been controversial [23,33,34,69,70].

$$\sigma_{eff}^{T} = p_c - p_p \tag{19}$$

where ${\sigma_{\text{eff}}}^{\text{T}}$ is the Terzaghi effective stress, p_{c} is the confining pressure, and p_{p} is the pore pressure. Some scholars have put forward several correction equations of effective stress, and the general model can be written as [69]

$$\sigma_{eff} = \sigma - \alpha p_p \tag{20}$$

where σ_{eff} is effective stress, σ is the external stress, α is the effective stress coefficient, $\varphi \leq \alpha \leq 1$, and φ is porosity [21,24,33,71–74]. It is certain that the value of α depends on the pore development degree of the porous medium, with which α increases [5,75]. When α is set at 1, σ_{eff} is the Terzaghi effective stress.

From Equation (20), we can see that the acting mechanisms on the coal matrix skeleton are obviously different between the external stress and the internal fluid pressure. In the confining pressure sensitivity experiment, the actual increment of total effective stress

suffered by coal is the absolute variation in the confining pressure (external stress) with the constant internal fluid pressure according to Equation (21). Under the condition of a non-adsorbing gas (e.g., He), the actual increment of total effective stress is generally less than the absolute variation in fluid pressure according to Equation (21). For an adsorbing gas such as CH_4, the actual total effective stress may increase first and then decrease during gas recovery simulation; nonetheless, it is generally lower than that under a non-adsorbing gas at the same reservoir fluid pressure. This is because methane desorption produces adsorption-induced equivalent tensile stress that negatively affects the total effective stress. As a result, the stress sensitivity damage to permeability in coal reservoirs becomes relatively weaker compared with the helium case. After the rebound pressure (p_{rb}) is reached in the low-pressure stage, the total effective stress begins to decrease and permeability rebounds. In the low- to ultra-low-pressure range, permeability may even recover to its original reservoir condition and continue to increase.

$$\Delta\sigma eff = \Delta\sigma - \alpha\Delta p_p \tag{21}$$

where $\Delta\sigma_{eff}{}^T$ is the effective stress increment; $\Delta\sigma$ is the external stress increment; Δp_p is the pore pressure change; and α is the effective stress coefficient.

Based on the above analysis, it can be concluded that the actual increment of total effective stress is relatively smaller by reducing the amount of He/CH_4 fluid pressure in comparison to the equivalent confining pressure sensitivity experiment; as a result, the permeability sensitivity to He/CH_4 fluid pressure shows the characteristics of lagging behind, and its damage degree is relatively weaker. In particular, CH_4 is expected to show the weakest permeability sensitivity damage among these scenarios because of the reverse-acting of the equivalent tensile stress induced by methane adsorption (p_{ad}).

In conclusion, confining pressure sensitivity experiments could effectively simulate the permeability sensitivity characteristic of coal to external geostress (e.g., overburden pressure) in an underground coal mining area. Meanwhile, pore/fluid pressure sensitivity experiments could effectively simulate the permeability sensitivity characteristic of coal to reservoir fluid pressure in a complex fluid–solid coupling area during actual CBM production. So, it is worth noting that using the gas originally contained in the reservoir for simulation experiments is of very important practical guiding significance for the underground reservoir itself. Hence, we would overestimate the actual damage degree of reservoir permeability during CBM production by using the experimental result of confining pressure sensitivity. And the pore/fluid pressure sensitivity experiment is more appropriate for evaluating the actual damage degree of reservoir permeability in the process of CBM recovery.

6.2. Determination Method of Effective Stress Coefficient

Many scholars have discussed the theoretical derivation and value of the effective stress coefficient (α), but there is not a unified understanding. One of the most famous calculation methods for the effective stress coefficient is based on the compressibility of porous rock and can be determined as follows [75–78]:

$$\alpha = 1 - \frac{K}{K_S} \tag{22}$$

where K is the bulk modulus of rock and K_S is the bulk modulus of the solid matrix/grain of rock. Some scholars even suggest that α is not always a constant and may be a variable depending on the stress environment [20,23,33,79,80]. Therefore, it is difficult to obtain the effective stress coefficient through mechanics experiments on rock. Moreover, the calculation of the effective stress coefficient is usually reported in sandstone [17,23,75],

shale [24], limestone [20], granite [19], etc. In view of the poor mechanical properties and gas adsorption of coal, there were few reports on its effective stress coefficient [5,21,51].

Stress sensitivity is the inherent nature of coal, and its behavior is controlled by the effective stress principle. Confining and pore pressures change effective stress in different ways. Therefore, the effective stress coefficient of coal can be calculated based on the two kinds of sensitivity experiments.

The negative exponential function relationship between coal permeability and effective stress could be expressed as

$$\ln(k/k_0) = -a\Delta\sigma_{eff} = -a\Delta\sigma = -a\alpha\Delta p = -a_p\Delta p \quad (23)$$

where k_0 is the original permeability of the coal reservoir, a is the sensitivity curve regression coefficient of the effective stress (or confining pressure), $\Delta\sigma_{eff}$ is the effective stress increment, $\Delta\sigma$ is the external stress increment, Δp is the pore pressure decrement, α is the effective stress coefficient, and a_p is the sensitivity curve regression coefficient of pore pressure.

The effective stress coefficient can be easily deduced as follows:

$$\alpha = a_p/a \quad (24)$$

Namely, α is the ratio of the sensitivity curve regression coefficient of pore pressure and the sensitivity curve regression coefficient of confining pressure. By fitting Equation (23), a for sample S1 and a_p for sample S3 are 0.976 and 0.499 MPa^{-1}, as presented in Figures 4 and 5. So, the effective stress coefficient of the coal studied is about 0.511. Thus, there would be a large error when we describe the fluid–solid coupling characteristics of the coal reservoir with the Terzaghi effective stress (i.e., α = 1). Zou et al. [21] have confirmed through experiments that it is relatively unreasonable to set the effective stress coefficient as unity for low permeability reservoirs such as coal. In addition, it is important to note that we should implement multi-group contrast experiments of the two sensitivities for a kind of coal, and the average value of the effective stress coefficient calculated may be closest to its true value. As a result, the permeability stress sensitivity experiment for the coal reservoir has provided a new method for calculating the actual numerical value of the effective stress coefficient of the coal reservoir.

6.3. Dynamic Evolution Characteristics of Coal Reservoir Permeability in the Study Area

For actual coal reservoirs, once their basic physical parameters are obtained, a dynamic permeability evolution model can be established and an accurate *k*–*p* curve can be constructed. This allows for a forward analysis of permeability evolution during CBM production as reservoir pressure gradually declines.

Taking the No. 3 coal seam, the main CBM production layer in the study area, as the research object, its basic physical parameters are summarized in Table 4. Compared with conventional natural gas reservoirs, CBM coal reservoirs exhibit characteristics of low pressure, low permeability, and low gas saturation. The relatively low critical desorption pressure indicates that the early stage of CBM production involves a long period of water drainage to reduce reservoir pressure. Only after the reservoir pressure declines to the critical desorption pressure does methane begin to desorb in large quantities.

Table 4. Basic physical parameters of 3# coal seam.

α	ρ/t/m^3	c_f/MPa^{-1}	ν	T/K	a/m^3/t	b/MPa^{-1}	V_a/m^3/t	p_0/MPa	p_{cd}/MPa	S_g/%	k_{0w} /$\times 10^{-3}$ μm^2
0.511	1.46	0.22	0.3	298	32.26	0.42	10	5	2.36	49.7	0.2

Note: The effective stress coefficient α (=0.511) is determined based on the method described in Section 6.3. p_0 is the original reservoir pressure; V_a is the measured gas content; p_{cd} is the critical desorption pressure; S_g is the gas saturation; k_{0w} is the original well test permeability of the coal reservoir in the study area.

Substituting the parameters listed in Table 4 into Equation (16) yields the dynamic permeability evolution model for the No. 3 coal reservoir in the study area.

The saturation and critical desorption pressure are calculated from the isothermal adsorption curve, as shown in Figure 9. The corresponding *k*–*p* curve during reservoir pressure decline is shown in Figure 8. The curve indicates that the permeability evolution can be divided into two stages separated by the critical desorption pressure. The first stage corresponds to a rapid permeability decline. The second stage corresponds to a slowed decline followed by a rebound.

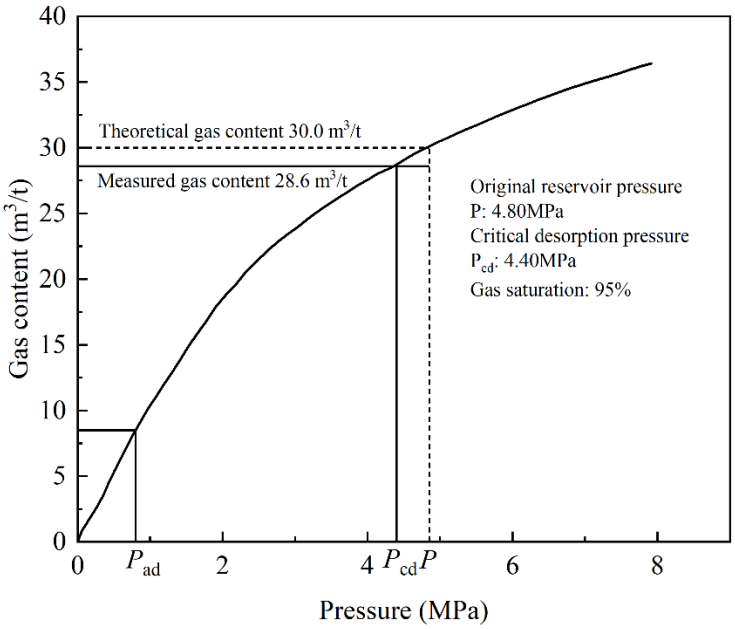


Figure 9. Saturation and critical desorption pressure are calculated from the isothermal adsorption curve.

During the first stage, CBM production mainly involves a prolonged drainage and depressurization process. Most methane remains adsorbed on coal pore surfaces, and only single-phase water flows out. The total effective stress increases monotonically as reservoir pressure decreases, resulting in a continuous rapid decline in permeability. Consequently, strong stress sensitivity damage inevitably occurs in this stage, as shown in Equation (16).

In the second stage, once the reservoir pressure drops below the critical desorption pressure, methane begins to desorb significantly. Matrix shrinkage induced by desorption and the increasing adsorption-induced tensile stress (p_{ad}) begin to act simultaneously. This causes the increasing trend of total effective stress to weaken, as shown in Equation (17). With further pressure decline, the total effective stress stops increasing and eventually decreases. Matrix shrinkage induced by gas desorption suppresses the continuous reduction in permeability. As a result, permeability first decreases more slowly to a minimum value and then begins to rebound. When the reservoir pressure reaches the rebound pressure (about 1.07 MPa), permeability stress sensitivity damage reaches its maximum and permeability reaches its minimum value (about 0.05 $\times$ 10^{-3} μm^2). Subsequently, perme-

ability gradually rebounds in the low-pressure stage, although the recovery amplitude is relatively small.

Overall, permeability stress sensitivity is strong during the early drainage stage but becomes weaker during the later gas production stage due to the self-regulating effect of the coal matrix. In theory, when reservoir pressure approaches zero, permeability may recover to approximately 0.06×10^{-3} μm^2.

Overall, significant stress sensitivity damage to permeability is unavoidable during depressurization in the CBM production process. Because both the critical desorption pressure and rebound pressure are relatively low, the self-regulating capacity of coal in the later stage is limited. Consequently, CBM development in the study area is characterized by a slow and long-term production process under low-pressure and low-permeability conditions.

It should be noted that all experiments in this study were conducted at room temperature (298 K), whereas the actual reservoir temperature in the study area (at a burial depth of approximately 500 m) is generally in the range of 25–40 °C. Temperature variations may influence gas adsorption behavior, coal matrix deformation, and the Langmuir parameters. In general, an increase in temperature tends to reduce gas adsorption capacity and weaken adsorption-induced swelling effects, which may consequently affect permeability evolution. Nevertheless, within this relatively moderate temperature range, the overall trends of permeability sensitivity and the fundamental fluid–solid coupling mechanisms are not expected to change significantly. Therefore, temperature is considered a potential source of uncertainty in this study.

6.4. Theoretical Verification of Permeability Sensitivity to Reservoir Pressure Based on Actual CBM Production Data

Overall, the #3 coal seam in this area is generally characterized by a large burial depth (between 700 m and 900 m) and a shallow initial dynamic liquid level depth; thus, the coal reservoir possesses a high water content and high original reservoir pressure. Gas wells typically undergo extensive drainage and pressure reduction operations before gas breakthrough, with dynamic liquid level drawdown consistently exceeding 400 m, resulting in generally low critical desorption pressures for the reservoirs. The overall gas production performance in this area is suboptimal, which is attributed to low gas saturation and permeability. We selected actual production data from Well 1-103, a representative well in the study area, to further validate the aforementioned theory regarding permeability sensitivity to reservoir pressure.

The actual drainage and production curve of Well 1-103 is shown in Figure 10. By comprehensively analyzing the dynamic liquid level decline curve, water production curve, and gas production curve, key information reflecting the dynamic changes in reservoir pressure and permeability can be obtained. During the initial stage, drainage and pressure reduction were maintained at a constant flow rate of approximately 3–4 m^3/d. After 125 days of drainage and pressure reduction, CBM gas production began to manifest significantly. At this point, the dynamic liquid level depth had dropped from an initial level of approximately 110 m to about 390 m. It was calculated that the pressure drop (P_{drop}) in the coal reservoir immediately adjacent to the wellbore was approximately 2.65 MPa. Consequently, the coal reservoir pressure at this moment equals the critical desorption pressure of 2.35 MPa (the difference between p_0 and P_{drop}), which is in excellent agreement with the critical desorption pressure (2.36 MPa) obtained from the aforementioned experiments.

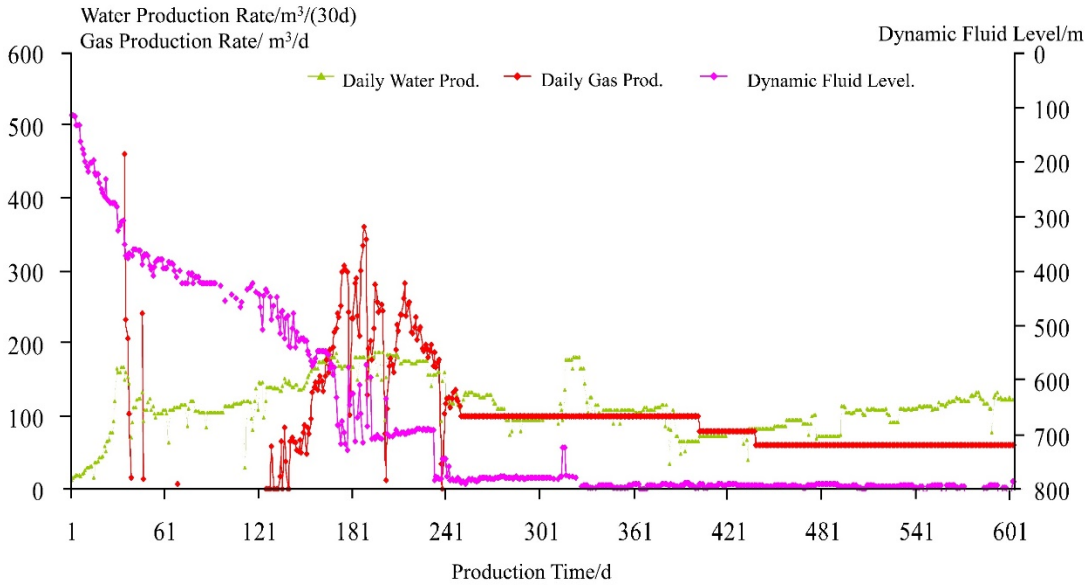


Figure 10. Actual drainage and production curve of Well 1-103.

After approximately 155 days of drainage and production, the well entered a period of rapid dynamic liquid level decline, with water production remaining at a consistently high level (approximately 6 m^3/d) and gas production increasing rapidly, entering a high-yield phase. Based on a comprehensive analysis, it can be determined that the 155-day mark represents the rebound node of the coal reservoir permeability. At this point, the dynamic liquid level dropped to approximately 510 m, and the pressure drop (P_{drop}) in the coal reservoir immediately adjacent to the wellbore was calculated to be approximately 4.0 MPa. Thus, the coal reservoir pressure at this time equals the permeability rebound pressure of 1.0 MPa (the difference between p_0 and P_{drop}), showing excellent agreement with the rebound pressure point (0.8–1.1 MPa) obtained via the aforementioned model.

It is evident that the previously constructed dynamic theoretical model, which describes coal reservoir permeability as a function of reservoir pressure during CBM drainage and production, can effectively capture the unique fluid (liquid, gas)–solid coupling characteristics of coal reservoirs. This practice indirectly validates the theory of coal reservoir permeability sensitivity to reservoir pressure and the rationality and accuracy of the calculation method for the effective stress coefficient. The theory presented in this paper can better serve the monitoring and prediction of drainage production and coal reservoir pressure systems.

7. Conclusions

Based on the unique fluid (gas, liquid)–solid coupling characteristics of coal reservoirs, a dynamic theoretical model of coal reservoir permeability, characterized by reservoir pressure, was constructed. Furthermore, the general characteristics of the stress sensitivity of coal permeability during CBM recovery were analyzed. The dynamic evolution characteristics of coal reservoir permeability in the study area were further analyzed. Using production data from a typical actual CBM production well in the study area as an example, the relevant theories regarding coal reservoir permeability sensitivity to reservoir pressure were validated in practice. This indirectly confirms the rationality and accuracy of the calculation method for the effective stress coefficient, which relies on laboratory coal permeability sensitivity simulation experiments. This study provides a robust theoretical foundation for the systematic monitoring and prediction of fluid output, coal reservoir pres-

sure, and permeability during the CBM production process, holding significant practical implications.

(1) The permeability sensitivity characteristics of coal reservoirs with respect to reservoir pressure can be reliably reproduced through pore pressure sensitivity experiments. A novel method for calculating the effective stress coefficient was proposed. Its value could be determined by computing the ratio of the regression coefficient from the pore pressure sensitivity curve to that from the confining pressure sensitivity curve.

(2) Based on the mechanistic analysis of fluid (liquid, gas)–solid coupling characteristics in coal reservoirs (see Section 5.2), a theoretical dynamic permeability model for the coal reservoir was derived (Equations (16) and (17)), through which the stress sensitivity of coal permeability during CBM recovery was systematically analyzed. In this process, the effective stress coefficient value of the coal reservoir can be obtained through reservoir permeability sensitivity experiments.

(3) Based on the dynamic permeability model, the dynamic evolution characteristics of coal reservoir permeability in the study area were discussed. Furthermore, by integrating data from a typical actual CBM production well in the study area, the feasibility of the dynamic theoretical model regarding coal reservoir permeability sensitivity to reservoir pressure, as well as the experimental calculation method for the effective stress coefficient value, was indirectly validated in practice. This holds significant theoretical and practical implications for achieving the precise monitoring and prediction of drainage production and coal reservoir pressure systems in the future.

Author Contributions: Conceptualization, X.X. Methodology and Writing—Original Draft Preparation; Y.X. Software, Q.L. Validation and Resources, S.Z. Formal Analysis, L.T. Investigation, Z.X. Data Curation. All authors have read and agreed to the published version of the manuscript.

Funding: This research was funded by the National Natural Science Foundation of China (grant numbers 41904118 and 42202210) and the Natural Science Foundation of Henan Province (grant number 262300420282).

Data Availability Statement: The original contributions presented in this study are included in the article. Further inquiries can be directed to the corresponding author.

Acknowledgments: The authors would like to acknowledge the experimental platform and technical support provided by the School of Energy Science and Engineering, Henan Polytechnic University.

Conflicts of Interest: The authors declare no conflicts of interest.

References

1. Clarkson, C.R. Production data analysis of unconventional gas wells: Review of theory and best practices. *Int. J. Coal Geol.* **2013**, *109*, 101–146. [CrossRef]
2. Meng, Z.; Peng, S.; Fu, J. Study on control factors of rock mechanics properties of coal-bearing formation. *Chin. J. Rock. Mech. Eng.* **2002**, *21*, 102–106.
3. Meng, Y.; Li, Z.P.; Lai, F.P. Experimental study on porosity and permeability of anthracite coal under different stresses. *J. Pet. Sci. Eng.* **2015**, *133*, 810–817. [CrossRef]
4. Puri, R.; Seidle, J.P. Measurement of Stress-Dependent Permeability in Coal and Its Influence on Coalbed Methane Production. *In Situ* **1992**, *16*, 183–202.
5. Chen, Z.W.; Pan, Z.J.; Liu, J.S.; Connell, L.D.; Elsworth, D. Effect of the effective stress coefficient and sorption-induced strain on the evolution of coal permeability: Experimental observations. *Int. J. Greenh. Gas. Control* **2011**, *5*, 1284–1293.
6. Wang, R.; Yue, X.A.; Zhao, R.B.; Yan, P.X.; Freeman, D. Effect of stress sensitivity on displacement efficiency in CO_2 flooding for fractured low permeability reservoirs. *Pet. Sci.* **2009**, *6*, 277–283. [CrossRef]
7. Dong, J.J.; Hsu, J.Y.; Wu, W.J.; Shimamoto, T.; Hung, J.H.; Yeh, E.C.; Wu, Y.H.; Sone, H. Stress-dependence of the permeability and porosity of sandstone and shale from TCDP Hole-A. *Int. J. Rock. Mech. Min.* **2010**, *47*, 1141–1157. [CrossRef]
8. McKee, C.R.; Bumb, A.C.; Koenig, R.A. Stress-dependent permeability and porosity of coal. In *International Coalbed Methane Symposium*; University of Alabama: Tuscaloosa, AL, USA, 1987; pp. 183–193.

9. Davies, J.P.; Davies, D.K. Stress-dependent permeability: Characterization and modeling. *Spe J.* **2001**, *6*, 224–235. [CrossRef]
10. Meng, Z.P.; Zhang, J.C.; Wang, R. In-situ stress, pore pressure and stress-dependent permeability in the Southern Qinshui Basin. *Int. J. Rock. Mech. Min.* **2011**, *48*, 122–131.
11. Tao, S.; Wang, Y.B.; Tang, D.Z.; Xu, H.; Lv, Y.M.; He, W.; Li, Y. Dynamic variation effects of coal permeability during the coalbed methane development process in the Qinshui Basin, China. *Int. J. Coal Geol.* **2012**, *93*, 16–22. [CrossRef]
12. Reucroft, P.J.; Patel, H. Gas-Induced Swelling in Coal. *Fuel* **1986**, *65*, 816–820. [CrossRef]
13. Jasinge, D.; Ranjith, P.G.; Choi, X.; Fernando, J. Investigation of the influence of coal swelling on permeability characteristics using natural brown coal and reconstituted brown coal specimens. *Energy* **2012**, *39*, 303–309. [CrossRef]
14. Connell, L.D.; Lu, M.; Pan, Z.J. An analytical coal permeability model for tri-axial strain and stress conditions. *Int. J. Coal Geol.* **2010**, *84*, 103–114. [CrossRef]
15. Mitra, A.; Harpalani, S.; Liu, S.M. Laboratory measurement and modeling of coal permeability with continued methane production: Part 1-Laboratory results. *Fuel* **2012**, *94*, 110–116. [CrossRef]
16. Meng, Z.P.; Hou, Q.L. Coupling model of stress-dependent permeability in high-rank coal reservoir and its control mechanism. *Chin. J. Geophys.* **2013**, *56*, 667–675.
17. Rathnaweera, T.D.; Ranjith, P.G.; Perera, M.S.A.; Yang, S.Q. Determination of effective stress parameters for effective CO_2 permeability in deep saline aquifers: An experimental study. *J. Nat. Gas. Sci. Eng.* **2015**, *24*, 64–79.
18. Bernabe, Y. The Effective Pressure Law for Permeability during Pore Pressure and Confining Pressure Cycling of Several Crystalline Rocks. *J. Geophys. Res.-Solid.* **1987**, *92*, 649–657. [CrossRef]
19. Morrow, C.A.; Zhang, B.C.; Byerlee, J.D. Effective Pressure Law for Permeability of Westerly Granite under Cyclic Loading. *J. Geophys. Res.-Solid* **1986**, *91*, 3870–3876. [CrossRef]
20. Ghabezloo, S.; Sulem, J.; Guedon, S.; Martineau, F. Effective stress law for the permeability of a limestone. *Int. J. Rock. Mech. Min.* **2009**, *46*, 297–306. [CrossRef]
21. Zou, J.P.; Chen, W.Z.; Yang, D.S.; Yu, H.D.; Yuan, J.Q. The impact of effective stress and gas slippage on coal permeability under cyclic loading. *J. Nat. Gas. Sci. Eng.* **2016**, *31*, 236–248. [CrossRef]
22. Tian, X.F.; Cheng, L.S.; Cao, R.Y.; Wang, Y.; Zhao, W.Q.; Yan, Y.Q.; Liu, H.J.; Mao, W.H.; Zhang, M.Y.; Guo, Q. A new approach to calculate permeability stress sensitivity in tight sandstone oil reservoirs considering micro-pore-throat structure. *J. Pet. Sci. Eng.* **2015**, *133*, 576–588. [CrossRef]
23. Li, M.; Xiao, W.L.; Bernabe, Y.; Zhao, J.Z. Nonlinear effective pressure law for permeability. *J. Geophys. Res.-Solid* **2014**, *119*, 302–318. [CrossRef]
24. Kwon, O.; Kronenberg, A.K.; Gangi, A.F.; Johnson, B. Permeability of Wilcox shale and its effective pressure law. *J. Geophys. Res.-Solid* **2001**, *106*, 19339–19353. [CrossRef]
25. Terzaghi, K.V. The shearing resistance of saturated soils and the angle between the planes of shear. In *Proceedings of the 1st International Conference on Soil Mechanics and Foundation Engineering*; Harvard University Press: Cambridge, MA, USA, 1936; pp. 54–56.
26. Connell, L.D.; Mazumder, S.; Sander, R.; Camilleri, M.; Pan, Z.J.; Heryanto, D. Laboratory characterisation of coal matrix shrinkage, cleat compressibility and the geomechanical properties determining reservoir permeability. *Fuel* **2016**, *165*, 499–512. [CrossRef]
27. Feng, R.M.; Harpalani, S.; Pandey, R. Laboratory measurement of stress-dependent coal permeability using pulse-decay technique and flow modeling with gas depletion. *Fuel* **2016**, *177*, 76–86. [CrossRef]
28. Li, Y.; Tang, D.Z.; Xu, H.; Meng, Y.J.; Li, J.Q. Experimental research on coal permeability: The roles of effective stress and gas slippage. *J. Nat. Gas. Sci. Eng.* **2014**, *21*, 481–488. [CrossRef]
29. Meng, Z.P.; Li, G.Q. Experimental research on the permeability of high-rank coal under a varying stress and its influencing factors. *Eng. Geol.* **2013**, *162*, 108–117. [CrossRef]
30. Chen, G.; Qin, Y.; Yang, Q.; Li, W.-Z. Different stress sensitivity of different coal rank reservoir permeability and its effect on the coalbed methane output. *J. China Coal Soc.* **2014**, *39*, 504–509.
31. Chen, Z.; Wang, Y.; Guo, K.; Sun, Q.; Zhang, Y. Stress sensitivity of high-rank coalbed methane reservoir. *Acta Geol. Sinca* **2008**, *82*, 1390–1395.
32. Li, C. A Study on the Stress Sensibility of Permeability of Reservoir Rocks. *Xinjiang Pet. Geol.* **2006**, *27*, 348–350.
33. Bernabe, Y. The Effective Pressure Law for Permeability in Chelmsford Granite and Barre Granite. *Int. J. Rock. Mech. Min.* **1986**, *23*, 267–275. [CrossRef]
34. Li, M.; Bernabe, Y.; Xiao, W.I.; Chen, Z.Y.; Liu, Z.Q. Effective pressure law for permeability of E-bei sandstones. *J. Geophys. Res.-Solid* **2009**, *114*, B07205. [CrossRef]
35. Hu, Y.; Yang, Y. A comparative study on drag reduction methods for continental shale drilling in the Fuxing Block, southeastern Sichuan Basin. *Reserv. Sci.* **2026**, *2*, 81–96. [CrossRef]

36. Palmer, I.; Mansoori, J. How permeability depends on stress and pore pressure in coalbeds: A new model. *SPE Reserv. Eval. Eng.* **1998**, *1*, 539–544. [CrossRef]
37. Cui, X.; Bustin, R.M. Volumetric strain associated with methane desorption and its impact on coalbed gas production from deep coal seams. *AAPG Bull.* **2005**, *89*, 1181–1202. [CrossRef]
38. Shi, J.; Durucan, S. Drawdown induced changes in permeability of coalbeds: A new interpretation of the reservoir response to primary recovery. *Transp. Porous Media* **2004**, *56*, 1–16. [CrossRef]
39. Pan, Z.; Connell, L.D. Modelling permeability for coal reservoirs: A review of analytical models and testing data. *Int. J. Coal Geol.* **2012**, *92*, 1–44. [CrossRef]
40. Liu, J.; Chen, Z.; Elsworth, D.; Miao, X.; Mao, X. Linking gas-sorption induced changes in coal permeability to directional strains through a modulus reduction ratio. *Int. J. Coal Geol.* **2010**, *83*, 21–30. [CrossRef]
41. Zeng, J.; Guo, J.; Liu, J.; Li, W.; Zhou, Y.; Tian, J. Anisotropic Permeability Model for Coal Considering Stress Sensitivity, Matrix Anisotropic Internal Swelling/Shrinkage, and Gas Rarefaction Effects. *Energy Fuels* **2023**, *37*, 2811–2832. [CrossRef]
42. Wang, Y.; Zhang, Q.; Zhu, W.; Wang, L.; Xie, G.; Liu, C.; Zou, X. Extension structural records in the Qinshui basin (North China) since the Late Mesozoic. *Int. J. Earth Sci.* **2014**, *103*, 2217–2232. [CrossRef]
43. Khan, M.; Nawaz, S.; Gao, X.; Khan, N.M. Reservoir Characterization of Eocene Carbonates and Cambrian Sands in the Eastern Potwar Region, Pakistan. *Reserv. Sci.* **2026**, *2*, 111–125. [CrossRef]
44. Xu, X.; Meng, Z.; Wang, Y. Experimental comparisons of multiscale pore structures between primary and disturbed coals and their effects on adsorption and seepage of coalbed methane. *J. Pet. Sci. Eng.* **2019**, *174*, 704–715. [CrossRef]
45. Chen, D.; Pan, Z.J.; Ye, Z.H.; Hou, B.; Wang, D.; Yuan, L. A unified permeability and effective stress relationship for porous and fractured reservoir rocks. *J. Nat. Gas Sci. Eng.* **2016**, *29*, 401–412. [CrossRef]
46. Warren, J.E.; Root, P.J. The Behavior of Naturally Fractured Reservoirs. *Soc. Pet. Eng. J.* **1963**, *3*, 245–255. [CrossRef]
47. Karacan, C.O.; Okandan, E. Fracture/cleat analysis of coals from Zonguldak Basin (northwestern Turkey) relative to the potential of coalbed methane production. *Int. J. Coal Geol.* **2000**, *44*, 109–125. [CrossRef]
48. *SY/T5336*; Chinese Petroleum Industry Standard. China Petroleum and Chemical Corporation Publishing House: Beijing, China, 2006.
49. Brace, W.F.; Walsh, J.B.; Frangos, W.T. Permeability of Granite under High Pressure. *J. Geophys. Res.* **1968**, *73*, 2225–2236. [CrossRef]
50. Zhang, R.; Ning, Z.F.; Yang, F.; Wang, X.; Zhao, H.W.; Wang, Q. Impacts of nanopore structure and elastic properties on stress-dependent permeability of gas shales. *J. Nat. Gas Sci. Eng.* **2015**, *26*, 1663–1672. [CrossRef]
51. St George, J.D.; Barakat, M.A. The change in effective stress associated with shrinkage from gas desorption in coal. *Int. J. Coal Geol.* **2001**, *45*, 105–113. [CrossRef]
52. Zhang, Y.H.; Xu, X.M.; Lebedev, M.; Sarmadivaleh, M.; Barifcani, A.; Iglauer, S. Multi-scale x-ray computed tomography analysis of coal microstructure and permeability changes as a function of effective stress. *Int. J. Coal Geol.* **2016**, *165*, 149–156. [CrossRef]
53. Jasinge, D.; Ranjith, P.G.; Choi, S.K. Effects of effective stress changes on permeability of latrobe valley brown coal. *Fuel* **2011**, *90*, 1292–1300. [CrossRef]
54. Tao, S. *Dynamic Variation Effects of Coal Reservoir Permeabillity and the Response of Gas Productivity in Southern Qinshui Basin*; China University of Geosciences: Beijing, China, 2011.
55. Tian, L.; Zhang, Q.; Li, X.; Li, C. Fracturing Effectiveness Evaluation Based on Flowback Data Using Pressure Transient Testing. *Reserv. Sci.* **2026**, *2*, 97–110. [CrossRef]
56. Wang, H.; Zhang, P.J.; Cheng, Y.Y.; Leng, Y.H.; Guo, C.Q.; Shi, H.D.; Wei, Z.J.; Liu, L.L.; Shi, L.Y.; Cheng, M.W.; et al. Evaluation of gas well productivity in low permeability gas reservoirs based on a modified back-pressure test method. *Pet. Explor. Dev.* **2014**, *41*, 500–503. [CrossRef]
57. Tek, M.R.; Grove, M.L.; Poettmann, F.H. Method for Predicting the Back-Pressure Behavior of Low Permeability Natural Gas Wells. *Trans. Am. I Min. Met. Eng.* **1957**, *210*, 302–309. [CrossRef]
58. Haymaker, E.R.; Binckley, C.W.; Burgess, F.R. Method of Establishing a Stabilized Back-Pressure Curve for Gas Wells Producing from Reservoirs of Extremely Low Permeability. *Trans. Am. I Min. Met. Eng.* **1949**, *186*, 71–82. [CrossRef]
59. Somerton, W.H.; Soylemezoglu, I.M.; Dudley, R.C. Effect of Stress on Permeability of Coal. *Int. J. Rock. Mech. Min. Sci. Géoméch. Abstr.* **1975**, *12*, 129–145. [CrossRef]
60. Enever, J.; Henning, A. The relationship between permeability and effective stress for Australian coal and its implications with respect to coalbed methane exploration and reservoir model. In *Proceedings of the 1997 International Coalbed Methane Symposium*; University of Alabama: Tuscaloosa, AL, USA, 1997.
61. *SY/T5358*; Chinese Petroleum Industry Standard. China Petroleum and Chemical Corporation Publishing House: Beijing, China, 2010.
62. Levine, J.R. Model study of the influence of matrix shrinkage on absolute permeability of coal bed reservoirs. *Geol. Soc. Lond. Spec. Publ.* **1996**, *109*, 197–212. [CrossRef]
63. Harpalani, S.; Schraufnagel, R.A. Shrinkage of coal matrix with release of gas and its impact on permeability of coal. *Fuel* **1990**, *69*, 551–556. [CrossRef]

64. Langmuir, I. The Constitution and Fundamental Properties of Solids and Liquids. Part I. Solids. *J. Am. Chem. Soc.* **1915**, *38*, 2221–2295. [CrossRef]
65. Seidle, J.; Huitt, L. Experimental Measurement of Coal Matrix Shrinkage Due to Gas Desorption and Implications for Cleat Permeability Increases. In Proceedings of the International Meeting on Petroleum Engineering, Beijing, China, 14–17 November 1995.
66. Adamson, A.W.; Gast, A.P. *Physical Chemistry of Surfaces*; John Wiley and Sons: Hoboken, NJ, USA, 1997.
67. Seidle, J.P.; Jeansonne, M.W.; Erickson, D.J. Application of Matchstick Geometry To Stress Dependent Permeability in Coals. In Proceedings of the SPE Rocky Mountain Regional Meeting, Casper, WY, USA, 18 May 1992.
68. Ttinger, I.L. Swelling stress in the gas-coal system as an energy source in the development of gas bursts. *Sov. Min. Sci.* **1979**, *15*, 494–501. [CrossRef]
69. Qiao, L.P.; Wong, R.C.K.; Aguilera, R.; Kantzas, A. Determination of Biot's Effective-Stress Coefficient for Permeability of Nikanassin Sandstone. *J. Can. Pet. Technol.* **2012**, *51*, 193–197. [CrossRef]
70. Zhang, K.; Zhou, H.; Hu, D.W.; Zhao, Y.; Feng, X.T. Theoretical Model of Effective Stress Coefficient for Rock/Soil-Like Porous Materials. *Acta Mech. Solida Sin.* **2009**, *22*, 251–260. [CrossRef]
71. Biot, M.A. General theory of three-dimensional consolidation. *J. Appl. Phys.* **1941**, *12*, 155–164. [CrossRef]
72. Han, G.; Dusseault, M.B. Description of fluid flow around a wellbore with stress-dependent porosity and permeability. *J. Pet. Sci. Eng.* **2003**, *40*, 1–16. [CrossRef]
73. Berryman, J.G. Exact effective-stress rules in rock mechanics. *Phys. Rev. A* **1992**, *46*, 3307–3311. [CrossRef]
74. Lade, P.V.; DeBoer, R. The concept of effective stress for soil, concrete and rock. *Geotechnique* **1997**, *47*, 61–78. [CrossRef]
75. Dassanayake, A.B.N.; Fujii, Y.; Fukuda, D.; Kodama, J. A new approach to evaluate effective stress coefficient for strength in Kimachi sandstone. *J. Pet. Sci. Eng.* **2015**, *131*, 70–79. [CrossRef]
76. Biot, M.; Willis, D. The theory of consolidation. *J. Appl. Elastic Coeff. Mech.* **1957**, *24*, 594–601. [CrossRef]
77. Nur, A.; Byerlee, J.D. An exact effective stress law for elastic deformation of rock with fluids. *J. Geophys. Res.* **1971**, *76*, 6414–6419. [CrossRef]
78. Robin, P.Y.F. Note on Effective Pressure. *J. Geophys. Res.* **1973**, *78*, 2434–2437. [CrossRef]
79. Gangi, A.F.; Carlson, R.L. An asperity-deformation model for effective pressure. *Tectonophysics* **1996**, *256*, 241–251. [CrossRef]
80. Prasad, M.; Manghnani, M.H. Effects of pore and differential pressure on compressional wave velocity and quality factor in Berea and Michigan sandstones. *Geophysics* **1997**, *62*, 1163–1176. [CrossRef]

Disclaimer/Publisher's Note: The statements, opinions and data contained in all publications are solely those of the individual author(s) and contributor(s) and not of MDPI and/or the editor(s). MDPI and/or the editor(s) disclaim responsibility for any injury to people or property resulting from any ideas, methods, instructions or products referred to in the content.